The influence of sodium and potassium dynamics on excitability, seizures, and the stability of persistent states: II. Network and glial dynamics

Ghanim Ullah[1], **John R. Cressman Jr.**[2], **Ernest Barreto**[2], and **Steven J. Schiff**[1,3]

[1]Center for Neural Engineering, Department of Engineering Science and Mechanics, The Pennsylvania State University, 212 Earth Engineering Science Building, University Park, PA 16802, USA, e-mail: ghanim@psu.edu

[2]Department of Physics and Astronomy, The Center for Neural Dynamics, and The Krasnow Institute for Advanced Study, George Mason University, Fairfax, VA 22030, USA

[3]Departments of Neurosurgery and Physics, The Pennsylvania State University, University Park, PA 16802, USA

Abstract

In these companion papers, we study how the interrelated dynamics of sodium and potassium affect the excitability of neurons, the occurrence of seizures, and the stability of persistent states of activity. We seek to study these dynamics with respect to the following compartments: neurons, glia, and extracellular space. We are particularly interested in the slower time-scale dynamics that determine overall excitability, and set the stage for transient episodes of persistent oscillations, working memory, or seizures. In this second of two companion papers, we present an ionic current network model composed of populations of Hodgkin–Huxley type excitatory and inhibitory neurons embedded within extracellular space and glia, in order to investigate the role of micro-environmental ionic dynamics on the stability of persistent activity. We show that these networks reproduce seizure-like activity if glial cells fail to maintain the proper micro-environmental conditions surrounding neurons, and produce several experimentally testable predictions. Our work suggests that the stability of persistent states to perturbation is set by glial activity, and that how the response to such perturbations decays or grows may be a critical factor in a variety of disparate transient phenomena such as working memory, burst firing in neonatal brain or spinal cord, up states, seizures, and cortical oscillations.

Keywords

Neuronal networks; Instability; Glia buffering; Seizures; Persistent activity

1 Introduction

Despite an extraordinary amount of interest in understanding the dynamics of seizures, we still lack a unifying dynamical definition of what a seizure is (Soltesz and Staley 2008). The extraordinary variety of experimental preparations and human epilepsies makes the quest for unifying principles especially difficult.

In the first of these two companion papers, we examined the role of potassium dynamics on the stability of the activity of a single neuron (Cressman et al. 2009). In this second of two papers, we apply our findings to the stability of networks of neurons. We undertake our study using the concept of "persistent states" of activity as a paradigm for our investigation. Increasing evidence points to the importance of persistent activity in the maintenance of mental state and working memory (Miller et al. 2003; Wang 2003). The maintenance of neural activity over time following an event has been observed experimentally in monkey prefrontal cortex during short-term working memory, i.e., delay periods of tasks that require the animals to remember certain features such as target location (Funahashi et al. 1989; Fuster 1995; Goldman-Rakic 1995; Miller et al. 1996; Rainer et al. 1998; Romo et al. 1999). The brain requires a certain degree of instability to form such an activity balance (often likened to a Turing instability (Murray 2003)). We here ask: what are the network properties that render such physiological persistent states stable to perturbations? and especially: what are the circumstances where such perturbations lead to seizure-like activity?

Synaptic interaction is in many systems the driver of persistent excitation. Neurons within a network may sustain activity by circulating activity among themselves, thus bypassing individual neurons' refractory periods. Such persistent network activity often requires a balance between inhibitory and excitatory activity (McCormick et al. 2003; Shu et al. 2003; Van Vreeswijk and Sompolinsky 1996). When inhibition is strong compared to excitation, the network responds to strong stimuli, but negative feedback suppresses the network such that the activity of all neurons decays with time. In intermediate conditions, where the excitation is balanced by inhibition, the network can exhibit a stable focus of activity (see for example Durstewitz et al. 2000; Vogels et al. 2005). This mode can be utilized in different kinds of information processing, for example to sustain a representation of spatial information for a period of time (Funahashi et al. 1989). When the network is dominated by excitation, the activity of all neurons can increase to a relatively high firing rate, and information processing by the network is impaired. For example, blocking $GABA_A$-receptor mediated inhibition can result in the transformation of recurrent persistent activity into intense epileptiform activity (Sanchez-Vives and McCormick 2000).

In most models of pathological conditions such as seizures, a shift from dominant (or balanced) inhibition to dominant excitation in a neuronal network is considered to be responsible for the network transition from the pre-ictal to ictal state (Trevelyan et al. 2006). In such conditions of imbalance between inhibition and excitation, moderate perturbations can drive a neuronal network from physiological to seizure-like activity. However, the conditions under which such network transitions occur in response to perturbations are not well known.

We hypothesize that perturbing an active neuronal network will reveal a dynamical signature of functional stability. We draw this analogy from the physics of equilibrium systems (Forster 1990). We suggest that such perturbation responses are an operational test of excitatory-inhibitory neuronal balance in neuronal networks.

We focus on the role that the extracellular space and glia may play in modulating the stability of these persistent states. Glial cells absorb excess ions, most importantly K^+, from the extracellular space and thus regulate excessive excitation due to decreased neuronal transmembrane K^+ gradients. Glia also release neuro-transmitters such as glutamate, which can cause excitation in the surrounding neurons through the activation of NMDA receptors (Parpura et al. 1994; Parpura and Haydon 2000; Tian et al. 2005). However, a characterization of how glial dysfunction affects the dynamics of neuronal network activity remains largely unstudied. For example, what would happen if the glial cells fail to adequately remove the excess K^+ ions from the interstitial volume or if they suddenly release excessive glutamate while the network is performing normally?

In recent work, there is gathering evidence characterizing the interplay between excitatory and inhibitory neurons during seizures (Fujiwara-Tsukamoto et al. 2004; Perez-Velazquez and Carlen 1999). Ziburkus et al. (2006) observed interplay between pyramidal cells (PCs) and interneurons (INs) during *in vitro* seizure-like events. In particular, PCs were seen go into a silent state when INs were burst firing, followed by burst firing in PCs when INs went to depolarization block. What might be the underlying network dynamics that can lead to such seizure patterns?

In this second of two companion papers we address these questions through mathematical modeling. We construct a physiologically-motivated model for the neuronal network that combines the Hodgkin-Huxley formalism for the neuronal ionic currents with a model for the dynamics of the extra- and intracellular K$^+$ concentrations ([K]) and includes glia and active ion pumps. We also include dynamic extra- and intracellular Na$^+$ concentration ([Na]). We show that this model is able to maintain localized, persistent activity when the glial network is functioning normally and excitation and inhibition are balanced. The model is then used to explore physiological conditions under which an otherwise normal network would show abnormal activity. We show that such networks reproduce seizure-like activity if glial cells fail to maintain the proper extracellular [K]. Our model builds upon the findings of a simplified single cell ionic micro-environmental model in the accompanying manuscript (Cressman et al. 2009).

2 Methods

A schematic of our model network is shown in Fig. 1.

2.1 Membrane potential dynamics

We used single-compartment neurons in a network consisting of 100 PCs and 100 INs. The equations governing the membrane potential of the PCs and INs are adopted from the model in (Gutkin et al. 2001), and are as follows.

$$
\begin{aligned}
C\frac{dV^{e/i}}{dt} &= I_{Na}^{e/i} + I_{K}^{e/i} + I_{L}^{e/i} + I_{syn}^{e/i} + I_{ext}^{e/i} + I_{rand}^{e/i} \\
I_{Na}^{e/i} &= -g_{Na}[m_{\infty}^{e/i}(V^{e/i})]^3 h^{e/i}\left(V^{e/i} - V_{Na}^{e/i}\right) \\
I_{K}^{e/i} &= -\left(g_{K}[n^{e/i}]^4 + \frac{g_{AHP}[Ca]_i^{e/i}}{1+[Ca]_i^{e/i}}\right)\left(V^{e/i} - V_{K}^{e/i}\right),
\end{aligned}
$$

(1)

where the superscript *e/i* refers to PC/IN (excitatory–inhibitory) cells in the network. Both intrinsic and synaptic ($I_{syn}^{e/i}$) currents are incorporated into the model neurons. The gating variables for the intrinsic currents are described in the companion paper (Cressman et al. 2009). The leak current used here is lumped and is given as

$$
I_{L}^{e/i} = -g_{L}\left(V^{e/i} - V_{L}^{e/i}\right).
$$

(2)

The slow calcium-activated K$^+$ current (the spike-frequency adapting or afterhyperpolarization current, g_{AHP}) is only included in the PCs, i.e. g_{AHP}=0 mS/cm^2 for INs. The various parameters and variables used in this paper are defined in Table 1.

In order to take into account the Ziburkus et al. (2006) findings of PC–IN interplay during seizure-like events, we modify the synaptic current entering the jth PC and IN from that used in (Gutkin et al. 2001). We use

$$I_{syn}^e = -\frac{(V_j^e - V_{ee})}{N} \sum_{k=1}^N g_{jk}^{ee} s_k^e \chi_{jk}^e - \frac{(V_j^e - V_{ie})}{N} \sum_{k=1}^N g_{jk}^{ie} s_k^i \chi_{jk}^i,$$

$$I_{syn}^i = -\frac{(V_j^i - V_{ei})}{N} \sum_{k=1}^N g_{jk}^{ei} s_k^e \chi_{jk}^e - \frac{(V_j^i - V_{ii})}{N} \sum_{k=1}^N g_{jk}^{ii} s_k^i \chi_{jk}^i,$$

(3)

where $V_j^{e/i}$ is the voltage of the jth excitatory–inhibitory neuron, $s_k^{e/i}$ is the variable giving the temporal evolution of the synaptic efficacy emanating from the kth excitatory–inhibitory neuron, and $\chi_{jk}^{e/i}$ takes into account the interplay between PCs and INs described above; that is, if a cell goes into depolarization block, then the synaptic inputs from that cell to others are reduced towards zero by the factor $\chi_{jk}^{e/i}$.

V_{ee}, V_{ei}, V_{ie}, and V_{ii} are the reversal potentials for the excitatory–excitatory, excitatory–inhibitory, inhibitory–excitatory, and inhibitory–inhibitory synaptic inputs, respectively. The subscripts ij in all equations in this paper represent the connection from cell i to cell j. The variables used in Eqs. (1)–(3) are given as

$$\tau^{e/i} \frac{ds^{e/i}}{dt} = \varphi \sigma(V^{e/i})(1 - s^{e/i}) - s^{e/i}$$
$$\sigma(V^{e/i}) = 1/[1 + \exp(-(V^{e/i} + 20)/4)]$$
$$g_{jk}^{ee} = \alpha_{ee} \sqrt{\frac{100}{\pi}} \exp\left(-100[(j-k)/N]^2\right)$$
$$g_{jk}^{ie} = \alpha_{ie} \sqrt{\frac{30}{\pi}} \exp\left(-30[(j-k)/N]^2\right)$$
$$g_{jk}^{ei/ii} = \alpha_{ei/ii} \sqrt{\frac{30}{\pi}} \exp\left(-30[(j-k)/N]^2\right)$$
$$\chi_{jk}^{e/i} = \begin{cases} \exp(-\eta^{e/i}/\upsilon) & \text{if} \quad \eta^{e/i} > 5.0 \\ 1 & \text{otherwise} \end{cases}$$
$$\frac{d\eta^{e/i}}{dt} = \gamma^{e/i}(V^{e/i} - V_b) - \tilde{\gamma}\,\eta^{e/i}$$
$$\gamma^{e/i} = \begin{cases} 0.4 & \text{if} \quad -30 < V^{e/i} < -10 \\ 0 & \text{otherwise} \end{cases}.$$

(4)

The parameter values used in Eqs. (1)–(4) are $\varphi=3$, $\tau^e= 4$ ms, $\tau^i=8$ ms, $g_L=0.05$ mS/cm^2, $V_{ee}=0$ mV, $V_{ie}=-80$ mV, $\alpha_{ie}=0.06$, $V_b=-50.0$ mV, $\tilde{\gamma}0.4$, $\upsilon=5.0$, $V_{ei}=0$ mV, and $V_{ii}=-80$ mV. The factors -100, -30, and -30 inside the exponential terms in the expressions for g_{jk}^{ee}, g_{jk}^{ie}, and $g_{jk}^{ei/ii}$, respectively, model the different spatial ranges of synaptic inputs made by the PCs and INs; thus, the PC-to-PC connections have a narrow spatial footprint, while the PC–IN and the IN–IN synaptic footprints are wider. $\chi_{jk}^{e/i}$ models the synaptic block due to depolarization, υ is an associated scale, $V^{e/i} \in [-30, -10]$, and $\eta^{e/i} > 5$ is the threshold to synaptic block due to depolarization.

Random currents ($I_{rand}^{e,i}$) are chosen from a uniform distribution over $[-10, 10]$, where both negative and positive pulses have equal arrival probability. A constant external current $I_{ext}^i = 0.5$ is injected into the INs. For simulations in this paper (unless otherwise mentioned), a spatially restricted stimulus of Gaussian form $I_{ext}^e = I_{amp} \exp(-60[(j - N/2)/N]^2)$ was injected

into PCs 21–79 at t=112 ms for 20 ms to induce the stable focus of activity, where N=100, j is neuron number and I_{amp} =1.5 (see also Gutkin et al. 2001). A value of α_{ii} =0.02 is used in all simulations.

2.2 Ion concentrations dynamics

The model also contains dynamic extra- and intracellular [K] and [Na], subject to the constraints in Cressman et al. (2009); see also Eqs. (8) and (9) below. The [K] in the interstitial volume surrounding each cell ($[K]_o$) was continuously updated based on K^+ currents across the neuronal membrane, Na^+–K^+ pumps, uptake by the glial network surrounding the neurons, and lateral diffusion of K^+ within the extracellular space. The $[K]_o$ dynamics is modeled by the following differential equation, which is modified from that in (Cressman et al. 2009) because of the network structure:

$$\frac{d[K]_o^{e/i}}{dt} = 0.33 I_k^{e/i} - 2\beta I_{pump}^{e/i} - I_{diff}^{e/i} - I_{glia}^{e/i} + \frac{D}{\Delta x^2}$$
$$\times \left([K]_{o(+)}^{e/i} + [K]_{o(-)}^{e/i} + [K]_o^{i/e} - 3[K]_o^{e/i} \right).$$

(5)

The factor β=7.0 corrects for the volume fraction between the interior of the cell and the extracellular space when calculating the concentration change and is based on (Mazel et al. 1998; McBain et al. 1990; Somjen 2004). $[K]_{o(+)}^{e/i}$ and $[K]_{o(-)}^{e/i}$ are the K^+ concentrations in the adjacent extracellular volumes corresponding to nearest neighbors in the same layer, $[K]_o^{i/e}$ is the K^+ concentration around the nearest neighbor in the second layer and mimics the K^+ diffusion across the layers, and D=2.5×10^{-6} cm^2/s is the diffusion coefficient for K^+ in water (Fisher et al. 1976). The factor 0.33 mM cm^2/μC in front of $I_K^{e/i}$ is used to convert the currents into ion concentration rate-of-change, and 2.0 in front of βI_{pump} is due to the fact that the Na^+-K^+ pump has an electrogenic 2:3 ratio. Further discussion of β and the 0.33 can be found in Appendix A from the companion paper Cressman et al. (2009).

The model also includes terms that replicate the effects of active pumps and diffusion through the surrounding glial network (Cressman et al. 2009). For pumps, we use

$$I_{pump}^{e/i} = \left(\frac{1.25}{1.0 + \exp\left((25.0 - [Na]_i^{e/i})/3.0 \right)} \right)$$
$$\times \left(\frac{1.0}{1.0 + \exp\left(8.0 - [K]_o^{e/i} \right)} \right).$$

(6)

The K^+ diffusion between the extracellular space and the bath solution is modeled by

$$I_{diff}^{e/i} = \varepsilon \left([K]_o^{e/i} - k_{o,\infty} \right),$$

and the glial uptake is modeled by

$$I_{glia}^{e/i} = - \frac{G_{glia}}{1.0 + \exp\left((18 - [K]_o^{e/i})/2.5 \right)},$$

(7)

where $k_{o,\infty}$ is the steady state K$^+$ concentration in the nearby reservoir—either the bath solution in a slice preparation, or the vasculature in the intact brain. Unless otherwise mentioned, a value of 1.3 s^{-1} for ε and 66.7 mM/s for G_{glia} is used throughout this paper, where G_{glia} is the glial buffering strength.

To complete the description of the [K] dynamics, we make the assumption that the flow of Na$^+$ into the cell is compensated by flow of K$^+$ out of the cell. Then the internal [K] ([K]$_i$) can be approximated by

$$[K]_i^{e/i} = 140.0 mM + \left(18.0 mM - [Na]_i^{e/i}\right),$$

(8)

where 140.0 and 18.0 mM respectively are the normal resting concentrations of K$^+$ and Na$^+$ inside the cell.

The internal and external Na$^+$ concentrations ([Na]$_i$, [Na]$_o$) are also updated in the model as

$$\frac{d[Na]_i^{e/i}}{dt} = 0.33 \frac{I_{Na}^{e/i}}{\beta} - 3 I_{pump}^{e/i}$$
$$[Na]_o^{e/i} = 144.0 mM - \beta \left([Na]_i^{e/i} - 18.0 mM\right),$$

(9)

where 144.0 mM in Eq. (9) is the normal resting extracellular Na$^+$ concentration. Further details on I_{pump}, I_{diff}, ε, G_{glia}, [K]$_i$, [Na]$_i$, and [Na]$_o$ can be found in Cressman et al. (2009).

The reversal potential for the leak current used in Eq. (2) is updated based on the instantaneous ion concentrations inside and outside the cell using the Goldman–Hodgkin–Katz equation

$$V_L^{e/i} = 26.64 \ln \left(\frac{[K]_o^{e/i} + 0.065 [Na]_o^{e/i} + 0.6 [Cl]_i^{e/i}}{[K]_i^{e/i} + 0.065 [Na]_i^{e/i} + 0.6 [Cl]_o^{e/i}} \right),$$

(10)

where $[Cl]_i^{e/i}$ and $[Cl]_o^{e/i}$ are the concentrations of intra- and extracellular chloride and are equal to 6.0 and 130 mM respectively.

2.3 Numerical integration

We integrated the model numerically using the fourth-order Runge–Kutta method with a time step of 0.01 ms. The spatial diffusion of [K]$_o$ was solved by the forward-difference method with a spatial grid Δx=10.0 μm; note also that the K$^+$ surrounding one cell (e.g. PC) can diffuse to the nearest neighbors in the same layer as well as the next layer (IN). Our results were robust to moderate changes in the ratio and number of PCs and INs. Code for our model is available from ModelDB.[1]

---

[1]http://senselab.med.yale.edu/modeldb/

3 Results

3.1 Persistent states

To study instability in neuronal networks, we investigated a two-layer composite of one-dimensional networks consisting of 100 PCs and 100 INs (see Fig. 1). Both neuron types were modeled as single-compartment conductance-based cells using the Hodgkin-Huxley formalism (Gutkin et al. 2001). The spike-frequency adapting current was only included in the PCs, a common property of these cells (Mason and Larkman 1990; Wang 1998). In the network, both cell types were connected among themselves (PC–PC and IN–IN) and to each other (PC–IN) through spatially-dependent synaptic profiles, where the average PC–PC connections are smaller than the others (IN–IN, PC–IN). Importantly, our model incorporates dynamic intra- and extracellular ion concentrations, along with the effects of pumps, glia, and diffusion. The details of the network connectivity and ion concentration dynamics are described in the "Methods" section.

We followed the protocol of Gutkin et al. (2001) to induce persistent activity in the network by applying a spatially localized Gaussian excitatory stimulus at time $t= 112$ ms for 20 ms. In response, the neurons exhibit discharge spikes that activate the connected neurons, which in turn activate other neurons. For an appropriate choice of synaptic parameters, this positive feedback leads to a self-sustained and spatially-localized activity which outlasts the input stimulus, as shown in Fig. 2(a). As in Fig. 3 of Gutkin et al. (2001), we find that this occurs when there is an appropriate balance between excitation and inhibition.

To clarify this notion, we examined the consequences of varying the overall strength of the PC–PC and the PC–IN synaptic strengths. Figure 2(b) shows plots of the synaptic parameters α_{ee} versus α_{ei} for three different values of the bath potassium concentration $k_{o,\infty}$. The region between the dark curves corresponds to parameter sets for which self-sustained and spatially-contained network activity can be observed. With too much excitation (i.e., in the region above the top curve), the activity spreads throughout the network. With too much inhibition (i.e., below the bottom curve), the network shows only transient activity in response to the stimulus. In the region between the curves, the excitation and inhibition are sufficiently balanced such that the stimulus gives rise to activity that is persistent and spatially restricted, such as that shown in Fig. 2(a).

We observed that the stability region shifts towards smaller values of α_{ee} when $k_{o,\infty}$ is increased (note the different vertical scales in the three panels of Fig. 2(b)). Thus, the increase in $[K]_o$ due to K^+ diffusion from the bath must be counterbalanced by a decrease in excitatory synaptic strength to maintain stability. Note also that the width of the stability region decreases with increasing $k_{o,\infty}$; we observed a 25% decrease in width as $k_{o,\infty}$ increased from 3 to 3.5 mM (Fig. 2(b)). These results are consistent with Figs. 3 and 8 of Oberheim et al. (2008), in which it was observed that in the epileptic brain, the density of spines and the volume of dendrites increases, which causes an increase in excitation. Meanwhile, the overlap of astrocytes and the increase in their volume enhances $[K]_o$ accumulation due to reduced extracellular space. This rearrangement reduces the glial network's capacity to buffer extracellular K^+ and contributes to increased glutamate release (Oberheim et al. 2008). The regions above the upper curves in Fig. 2(b) correspond to such a state.

We also investigated the stability of persistent activity by applying perturbing stimuli. Following Gutkin et al. (2001), we observed that persistent activity can be 'turned off' by a strong excitatory stimulus (see Fig. 2(a) at t=500 ms). We then applied more moderate stimuli to persistent activity generated with networks within the stable regions of Fig. 2(b). The thin lines inside each stability region demarcate the upper bound of the region that is stable to moderate perturbations. More precisely, if the network is between the lower bound of the region

and the thin line, then the network is stable to moderate perturbations (see also the discussion of Fig. 3(c) below). Analogous to the experimental results described above, our model shows that the network is less resistant to epileptic drive when already in a relatively excited state (contrast the three panels of Fig. 2(b)).

Persistent activity can only be initiated using a limited range of input current values (Fig. 2 (c)). If I_{amp} is too small, the combined effects of the stimulus and excitatory synaptic activity are not sufficient to cause a persistent state. Excessively high input current, I_{amp} is also ineffective at producing long-lasting behavior, as it shuts down the network by synchronizing the activity of all the neurons (e.g. Fig. 2(a)). There is also an intermediate range of I_{amp} values where the network activity spreads over all of the neurons. So in order of increasing stimulus strength, one can see the following four behaviors in the network (results not illustrated): (1) Transient behavior where the activity decays with time (below the lower range of the regions in Fig. 2(c)), (2) a stable focus of activity that lasts for several seconds (within the regions illustrated in Fig. 2(c)), (3) a state where the activity spreads throughout the network (above the upper range of the regions in Fig. 2(c)), and (4) a state with no activity where the current synchronizes and stops the activity of all neurons in the network (further to the right of the activity regions shown in Fig. 2(c)). We note that the experimental work of Pinto et al. (2005, Fig. 2 of this reference) is also consistent with these observations; in that study, a stimulus threshold for wave initiation and its dependence on inhibition and excitation was described.

3.2 Transition from persistent states to seizures

To examine the stability of persistent activity against perturbations, we plot the activity of the network for various values of α_{ee} using the same $k_{o,\infty}$=3.0 mM. We estimate the activity of the network by counting the number of spikes in the excitatory (PC) population that occur within 50 ms non-overlapping time windows, and calculating the average (spikes per millisecond). We take the value of α_{ee} such that it either lies at the boundary or within the region where we see a stable focus of activity (shown in Fig. 2(b), left panel). An initial excitatory stimulus (at t=112 ms for 20 ms) causes a stable focus of activity to appear. After some time, we apply a second stimulus (at t=500 ms for 20 ms) to all neurons in the network. The second stimulus is stronger than the first so that it can recruit all neurons in the network. As shown in Fig. 3(a), (b), we observe different behaviors depending on the value of α_{ee}. Inhibition dominates at smaller α_{ee} (0.214) and the excitatory perturbation causes the network to decay to silence as demonstrated through the raster plot in Fig. 3(a). For α_{ee} values within (0.215–0.216), the network returns to the spatially restricted persistent activity that was present before the perturbation. However, for larger α_{ee} (0.217), the network fails to regain its stable focus of activity and all the cells in the network persistently fire action potentials (Fig. 3(b)). The stability of a network persistent state depends on the balance of excitatory and inhibitory synaptic strength of the network. Consistent with our findings, Pinto et al. (2005) found that the permeability of cortical slices to epileptic wave initiation and spreading decreased by increasing 6,7-dinitroquinoxaline-2,3-dione (AMPA receptor antagonist). An opposite effect was observed by raising the picrotoxin (GABA$_A$ receptor antagonist) concentration (see for example Figs. 5 and 6 of Pinto et al. 2005).

As mentioned above, stability can be maintained after increasing $k_{o,\infty}$ by reducing the excitability in the network. Increasing $k_{o,\infty}$ leads to increases in the local potassium concentration $[K]_o$. In order to investigate how this effects stability, we repeated the simulations in Fig. 3(b) using three different values of $k_{o,\infty}$ (different $[K]_o$ values can also be achieved by varying the glial buffering strength G_{glia}, however, the results of these simulations remain unchanged). The values of α_{ee} are chosen such that they are always at the center of the three stability regions shown in Fig. 2(b). It is clear from Fig. 3(c) that for low $k_{o,\infty}$ values (3.0–3.5

mM), the activity of the network drops back to the level observed prior to the perturbation. However, the network is unable to regain its stable focus of activity after perturbation when $k_{o,\infty}$ is higher (4.0 mM). As mentioned earlier, the region of stability shrinks with increased $[K]_o$. At the same time the percentage of the activity region that is stable to perturbation also decreases with increasing $k_{o,\infty}$. In other words, for about 80% of the activity region for $k_{o,\infty}$ =3.0 mM in Fig. 2(b) (from lower bound to the thin solid line with bullets), the network activity is stable to perturbations of moderate size. When $k_{o,\infty}$ =3.5 mM and 4.0 mM, the network is stable only for about 50% and 30% (between thin solid line with bullets and lower bound) of the persistent activity regions respectively (see Fig. 2(b)). We note that in experimental work, an accelerated spread of epilepsy has been observed by elevating K^+ in the bath solution (Figs. 2 and 3 of Konnerth et al. 1984).

Recently, several groups have reported that the Ca^{2+} dependent glutamate release from glial cells generates slow transient inward currents in nearby neurons through the activation of NMDA receptors (Parpura et al. 1994; Parpura and Haydon 2000). These discoveries of neuron-glia interaction have been extended by Tian et al. (2005) and Kang et al. (2005) to glial contributions to epilepsy. They showed that glial cells appear to be capable of synchronizing the activity of adjacent neurons through simultaneous non-synaptic slow inward neuronal currents. Another group has made a contrasting claim that glutamate released by glia is not necessary for the generation of epileptic activity in hippocampal slices (Fellin et al. 2006). We use our computational model to differentiate the conditions under which the glial-based perturbations would cause the neuronal network to go to a seizure-like state from that where the glial perturbations are insufficient for the network to make the transition from normal to seizure-like state.

In the framework of our model, the net effect of glutamate released by glial cells will manifest itself as an increased excitatory synaptic drive (α_{ee}) in the network. To test the robustness of the network against glial induced excitability, we began our simulation with normal network activity as previously described. After establishing a stable focus of activity we increased the excitability of the network by increasing α_{ee} above the region of stable activity for 30 ms (i.e. we applied a second stimulus in α_{ee}). The abrupt increase in α_{ee} thus mimics the effect of sudden glutamate release from glia. The activity of the network spread throughout the network but whether or not the persistent state could be reestablished depended on the baseline value of α_{ee}. The network is stable to this perturbation for baseline values of α_{ee}=0.215–0.216 (Fig. 4). However, the rate at which the network restored its stable focus of activity depends on the baseline α_{ee} value. If the baseline value of α_{ee} is too small ($\leq$ 0.214), the transient α_{ee} increase destroys the persistent state. Similarly, for sufficiently large α_{ee} values the network was unable to restore its stable focus of activity and the analogue of epileptiform spread following perturbation is shown in the upper trace of Fig. 4 (analogous to Figs. 4 and 5 of Tian et al. (2005), where they observed epileptiform activity caused by increased excitation due to Ca^{2+} dependent glutamate release by glia). This behavior also depends on the extracellular K^+ concentration. For higher $[K]_o$ ($[K]_o \geq$4.0 mM) values the network cannot reestablish its stable activity when the excitability is increased and then restored (result not shown).

3.3 Spontaneous seizures in the network

Next we investigated the dynamics of the network as $[K]_o$ evolves in time. Since the K^+ dynamics is very slow we simulated the network for longer times. For the simulation in Fig. 5 (a)–(c), $k_{o,\infty}$ is taken equal to 14.0 mM, which generates very slow oscillations in $[K]_o$ (see Cressman et al. 2009). In Fig. 5(a) we show the membrane potential for one PC in the network. Initially the cell is silent when $[K]_o$ is low (Fig. 5(b)). However, as $[K]_o$ rises, the cell starts seizure-like tonic firing. The firing frequency increases as $[K]_o$ increases, followed by depolarization block. The spiking returns when $[K]_o$ starts decreasing. The cell eventually goes

to a silent state after $[K]_o$ has fallen below a certain value and the whole process repeats for the next cycle of $[K]_o$. The locking of the cells into depolarization block has been observed in experiments (Fig. 2 of Bikson et al. 2003; Fig. 2 of Ziburkus et al. 2006) and in simulation (Fig. 3 of Kager et al. 2007). This effect has been shown to quench synaptic transmission and could underlie the interplay seen between PC and IN during *in vitro* seizures if inhibition is differentially lost through depolarization block (Fig. 2 of Ziburkus et al. 2006). In Fig. 5(b) we show the traces for $[K]_o$ and $[Na]_i$, while the excitatory activity of the network is shown in Fig. 5(c). The activity drops to zero at higher $[K]_o$ values when the whole network transiently goes into depolarization block. In this slow time-scale setting the intervals between seizures are similar to that seen in seizure experiments (Fig. 2 of Ziburkus et al. 2006). Long-time scale intervals with network refractoriness have been also observed in cortical oscillations (Huang et al. 2004), neonatal burst firing (Leinekugel et al. 2002), spinal cord burst firing (Chub et al. 2006), up states (Shu et al. 2003), and interestingly in spreading depression (Somjen 2004; Kager et al. 2000).

After enhancing the glial uptake slightly (compared to the simulation in Fig. 5(a)–(c)) depolarization block disappears and all the neurons in the network show high frequency, lower amplitude seizure-like spiking when $[K]_o$ reaches a sufficiently high value during $[K]_o$ oscillations (Fig. 5(d),(e)). Like the previous example, each cell starts with slow spiking initially as $[K]_o$ starts rising (Fig. 5 dA) followed by rapid tonic firing at high $[K]_o$ (Fig. 5 dB). Finally, the network switches to a silent state as $[K]_o$ slowly falls to lower values (end of Fig. 5 dC) until the next cycle. In Fig. 5(e), we show $[K]_o$ and $[Na]_i$ for the same PC shown in Fig. 5(d). The increases in $[K]_o$ during seizures have been observed in other studies (Bazhenov et al. 2004; Fig. 1 of Bikson et al. 2003; Frohlich et al. 2008; Fig. 8 of Kager et al. 2000; Kager et al. 2007). The activity diagram (Fig. 5(f)) shows a clear peak at high $[K]_o$ values indicating increased but still partial (notice that the activity does not rise to 100 during seizures) spiking synchrony in the network. However, the longer time-scale oscillations (seizure episodes and $[K]_o$ oscillations) are more synchronized through the entire network. In Fig. 5 dD we show a raster plot for the network near the peak $[K]_o$ value during the cycle described above. The network shows a stable focus of activity for smaller $[K]_o$ values, which changes into seizure-like behavior for larger $[K]_o$ values (Fig. 5(f)), and interestingly is asynchronous, consistent with experimental (Figs. 11 and 12 of Netoff and Schiff 2002) and theoretical (Fig. 2 of Gutkin et al. 2001) findings.

4 Discussion

We have used a one-dimensional two-layer network model to study the physiological conditions under which a neuronal network can switch to a persistent state of activity, and the stability of the persistent state to perturbations. Previously, several experimental and theoretical studies have shown that spatially localized persistent activity in neuronal networks requires a balance between excitatory and inhibitory synaptic inputs (Compte et al. 2000; Funahashi et al. 1989; Gutkin et al. 2001). We show that the network not only needs balanced excitatory and inhibitory synaptic footprints, but also balanced levels of extracellular K^+, controlled by the glial syncytium, to achieve local persistent activity that is stable to perturbations.

Our study successfully models persistent activity during both the up state (Sanchez-Vives and McCormick 2000), and during the delay periods of working memory tasks using recurrent excitation balanced by local inhibition (Compte et al. 2000; Gutkin et al. 2001; Wang 1999). The persistent activity in our model can last for several seconds which has been observed in several experimental preparations (Fuster 1995; McCormick et al. 2003). In addition, the firing rate of our model PCs during the persistent activity is similar to that seen during the delay responses in memory tasks *in vivo* (Funahashi et al. 1989; Miller et al. 1996).

In recent years, neuroscience research has unveiled an unexpected complexity of glial cells. Astrocytes, in particular have been shown to affect virtually every aspect of neuronal function through glia-neuron cross talk. They have the ability to buffer excitatory ions such as K^+ from the interstitial volume (Amzica et al. 2002), preventing an undue increase in excitation of the neuronal network. They can also enhance the excitability of the network by releasing glutamate and ATP in a Ca^{2+} dependent manner, which can activate NMDA and AMPA receptors synaptically and non-synaptically (Parpura et al. 1994; Parpura and Haydon 2000). In spite of a direct role of glia in the activity modulation of neuronal networks, detailed models of glia-neuron interaction are few (Nadkarni and Jung 2003). Here we use a model to show that dysfunction of glial cells can cause the transition from normal stable neuronal activity to seizure-like uncontrolled activity. Several experimental studies support glial dysfunction during epileptic seizures (Heinemann et al. 2000; Hinterkeuser et al. 2000). Our results support exploring therapeutic manipulations targeting glial function in regulating pathological activity such as seizures.

The ability of astrocytes to release glutamate in a Ca^{2+} dependent manner has been recently extended by two groups to the glial bases of epilepsy (Tian et al. 2005; Kang et al. 2005). We tested the stability of the network to glial-induced excitatory perturbations by perturbing the network from its stable focus of activity by briefly raising the excitatory weight of the network. Our simulation shows that the ability of glial cells to induce seizure-like activity depends on the initial baseline state of the network. If the network is in a relatively low excitatory state, then a transient glial glutamate perturbation would not be able to cause epileptic activity no matter how strong the perturbations are. However, even a small perturbation by glial cells is enough to cause seizure-like activity in the network if its excitability set point is sufficiently high.

Recent experimental results point to the role of astrocytic domain reorganization in the epileptic brain (Oberheim et al. 2008). To test the effect of realistic spatial arrangements of glia, spatially explicit models are needed. Such models would have to take into account the effect of extracellular tortuosity and explicit molecular diffusion between network elements, something beyond the scope of the present study.

There is an extensive literature that describes the stability of ensemble systems (Forster 1990), and indeed the fundamental hallmark of a stable (equilibrium) system in physics is reflected in how such systems handle fluctuations. We hypothesize that an analogous principle regarding the response to perturbations applies to characterize the stability of biological systems. We therefore examined the response of our extended network of INs and PCs to fluctuations. First we delivered a perturbation that created a persistently active state and then delivered a second perturbation. Depending upon the excitability of the network, which we could set through the synaptic efficacy (Fig. 3(b)), or the extracellular K^+ level (Fig. 3(c)), the response of the persistent state to the second perturbation was either exponential decay back to the persistent state, a runaway expansion of activity to break through the inhibitory constraints and involve more of or the whole network, or destruction of the persistent state with quiescence (behaviors illustrated in Fig. 3(b),(c)). Such competition between excitation and inhibition in response to perturbation appears to be reflected in an 'inhibitory veto' in such networks in cortex (Trevelyan et al. 2006).

Our findings are an extension of previous model studies that demonstrated bistable states in networks, i.e., to fulfill the working memory function, these models have found the physiological conditions under which the network can switch back and forth between a resting state and spatially structured activity induced by transient inputs (see for example Compte et al. 2000). We extended these findings to identify the conditions under which a network displaying stable persistent activity can switch to seizure-like states. The maintenance of a low

$[K]_o$ is crucial to create persistent activity robust to perturbations. The K^+ mediated modulation described here likely will affect synaptic plasticity and homeostasis (Marder and Prinz 2002; Turrigiano 2008), and this warrants further investigation.

Neurophysiological studies of working memory by Miller et al. (1996) have shown that the delay activity in the prefrontal cortex of monkeys is resistant to occasional distractions. Through mathematical modeling these results were confirmed by Compte et al. (2000). This latter study related the distraction-resistant activity to the stimulus strength; that is, the activity packet was predicted to be resistant to small perturbations. The main finding of our study is that the network activity packet is stable provided that (1) the excitable synaptic strength is not too high (a parameter modulated by glial glutamate release); (2) $[K]_o$ is low enough to be within the physiological range (i.e. the glial network buffer is functioning properly); and (3) the perturbations are not too strong. Thus our study asserts two additional conditions on the stability of the neuronal activity. Even small perturbations can push the network to an unstable state if the network is already in a state of increased α_{ee} or the $[K]_o$ is relatively high. *Both of these conditions are regulated by a properly functioning glial network.*

The evolution of activity seen in Fig. 5(a),(d) is intimately linked to the ionic dynamics shown in Fig. 5(b),(e). Without incorporating such ionic and glial dynamics, such evolution would not appear. Seizure patterns, whether observed *in vitro* (Ziburkus et al. 2006), or from human patients recorded from scalp or intracranial electrodes (Schiff et al. 2005), demonstrate a prominent and very consistent evolution from initiation to termination. Whether such evolution observed from such different scales of experimental observation is related to the ionic and glial dynamics studied here is an intriguing question that warrants further exploration.

Although brains are not equilibrium systems, we propose that how neuronal networks respond to perturbations, and how the response to such perturbations decays (or grows), are critical determinants of the state of the brain, with parallels to other physical systems (Forster 1990). How neuronal networks respond to perturbations determines how transient patterns of activity emerge from background activity in response to internal fluctuations of activity or external stimuli. We propose that the response of a balanced, or mildly imbalanced network, to such perturbations is a fundamental feature which may underlie a variety of disparate transient phenomena such as seizures, working memory, up states, cortical oscillations, and spinal cord and hippocampal neonatal burst firing.

Acknowledgments

References

Amzica F, Massimini M, Manfridi A. Spatial buffering during slow and paroxysmal sleep oscillations in cortical networks of glial cells *in vivo*. Journal of Neuroscience 2002;22(3):1042–1053. [PubMed: 11826133]

Bazhenov M, Timofeev I, Steriade M, Sejnowski TJ. Potassium model for slow (2–3 Hz) *in vivo* neocortical paroxysmal oscillations. Journal of Neurophysiology 2004;92:1116–1132. [PubMed: 15056684]

Bikson M, Hahn PJ, Fox JE, Jefferys JGR. Depolarization block of neurons during maintenance of electro-graphic seizures. Journal of Neurophysiology 2003;90(4):2402–2408. [PubMed: 12801897]

Chub N, Mentis ZG, O'Donovan JM. Chloride-sensitive MEQ fluorescence in chick embryo motoneurons following manipulations of chloride and during spontaneous network activity. Journal of Neurophysiology 2006;95:323–330. [PubMed: 16192339]

Compte A, Brunel N, Goldman-Rakic PS, Wang XJ. Synaptic mechanisms and network dynamics underlying spatial working memory in a cortical network model. Cerebral Cortex 2000;10(9):910–923. [PubMed: 10982751]

Cressman JR, Ullah G, Ziburkus J, Schiff SJ, Barreto E. The influence of sodium and potassium dynamics on excitability, seizures, and the stability of persistent states: I. Single neuron dynamics. Journal of Computational Neuroscience. 200910.1007/s10827-008-0132-4

Durstewitz D, Seamans JK, Sejnowski TJ. Neuro-computational models of working memory. Nature Neuroscience 2000;3:1184–1191.

Fellin T, Gomez-Gonzalo M, Gobbo S, Carmignoto G, Haydon PG. Astrocytic glutamate is not necessary for the generation of epileptiform neuronal activity in hippocampal slices. Journal of Neuroscience 2006;26(36):9312–9322. [PubMed: 16957087]

Fisher RS, Pedley TA, Prince DA. Kinetics of potassium movement in norman cortex. Brain Research 1976;101(2):223–237. [PubMed: 1244970]

Forster, D. Hydrodynamic fluctuations, broken symmetry, and correlation. Boulder: Westview; 1990.

Frohlich, F.; Timofeev, I.; Sejnowski, TJ.; Bazhenov, M. Extracellular potassium dynamics and epileptogenesis. In: Soltesz, I.; Staley, K., editors. Computational neuroscience in epilepsy. Amsterdam: Academic; 2008.

Fujiwara-Tsukamoto Y, Isomura Y, Kaneda K, Takada M. Synaptic interactions between pyramidal cells and interneuron subtypes during seizure-like activity in the rat hippocampus. Journal of Physiology 2004;557(3):961–979. [PubMed: 15107470]

Funahashi S, Bruce CJ, Goldman-Rakic PS. Mnemonic coding of visual space in the monkey's dorsolateral prefrontal cortex. Journal of Neurophysiology 1989;61(2):331–349. [PubMed: 2918358]

Fuster, JM. Memory in the cerebral cortex. Cambridge: MIT; 1995.

Goldman-Rakic PS. Cellular basis of working memory. Neuron 1995;14(3):477–485. [PubMed: 7695894]

Gutkin BS, Laing CR, Colby CL, Chow CC, Ermentrout GB. Turning on and off with excitation: the role of spike-timing asynchrony and synchrony in sustained neural activity. Journal of Computational Neuroscience 2001;11(2):121–134. [PubMed: 11717529]

Heinemann U, Gabriel S, Jauch R, Schulze K, Kivi A, Eilers A, et al. Alterations of glial cell function in temporal lobe epilepsy. Epilepsia 2000;41(Suppl 6):S185–S189. [PubMed: 10999542]

Hinterkeuser S, Schroder W, Hager G, Seifert G, Blumcke I, Elger CE, et al. Astrocytes in the hippocampus of patients with temporal lobe epilepsy display changes in potassium conductances. European Journal of Neuroscience 2000;12(6):2087–2096. [PubMed: 10886348]

Huang X, Troy WC, Yang Q, Ma H, Laing CR, Schiff SJ, et al. Spiral waves in disinhibited mammalian neocortex. Journal of Neuroscience 2004;24:9897–9902. [PubMed: 15525774]

Kager H, Wadman JW, Somjen GG. Simulated seizures and spreading depression in a neuron model incorporating interstitial space and ion concentrations. Journal of Neurophysiology 2000;84:495–512. [PubMed: 10899222]

Kager H, Wadman JW, Somjen GG. Seizure-like afterdischarges simulated in a model neuron. Journal of Computational Neuroscience 2007;22:105–128. [PubMed: 17053996]

Kang N, Xu J, Xu Q, Nedergaard M, Kang J. Astrocytic glutamate release-induced transient depolarization and epileptiform discharges in hippocampal CA1 pyramidal neurons. Journal of Neurophysiology 2005;94(6):4121–4130. [PubMed: 16162834]

Konnerth A, Heinemann U, Yaari Y. Slow transmission of neural activity in hippocampal area CA1 in absence of active chemical synapses. Nature 1984;307:69–71. [PubMed: 6318119]

Leinekugel X, Khazipov R, Cannon R, Hirase H, Ben-Ari Y, Buzsaki G. Correlated bursts of activity in the neonatal hippocampus *in vivo*. Science 2002;298(5575):2049–2052. [PubMed: 12065842]

Marder E, Prinz AA. Modulating stability in neuron and network function: The role of activity in homeostasis. BioEssays 2002;24:1145–1154. [PubMed: 12447979]

Mason A, Larkman A. Correlations between morphology and electrophysiology of pyramidal neurons in slices of rat visual cortex. II. Electrophysiology. Journal of Neuroscience 1990;10(5):1415–1428. [PubMed: 2332788]

Mazel T, Simonova Z, Sykova E. Diffusion heterogeneity and anisotropy in rat hippocampus. Neuroreport 1998;9(7):1299–1304. [PubMed: 9631417]

McBain CJ, Traynelis SF, Dingledine R. Regional variation of extracellular space in the hippocampus. Science 1990;249(4969):674–677. [PubMed: 2382142]

McCormick DA, Shu Y, Hasenstaub A, Sanchez-Vives M, Badoual M, Bal T. Persistent cortical activity: Mechanisms of generation and effects on neuronal excitability. Cerebral Cortex 2003;13:1219–1231. [PubMed: 14576213]

Miller EK, Erickson CA, Desimone R. Neural mechanisms of visual working memory in prefrontal cortex of the macaque. Journal of Neuroscience 1996;16(16):5154–5167. [PubMed: 8756444]

Miller P, Brody CD, Romo R, Wang XJ. A recurrent network model of somatosensory parametric working memory in the prefrontal cortex. Cerebral Cortex 2003;13:1208–1218. [PubMed: 14576212]

Murray, JD. Mathematical Biology II: Spatial models and biomedical applications. New York: Springer; 2003.

Nadkarni S, Jung P. Spontaneous oscillations of dressed neurons: A new mechanism for epilepsy? Physical Review Letters 2003;91(268101):1–4.

Netoff TI, Schiff SJ. Decreased neuronal synchronization during experimental seizures. Journal of Neuroscience 2002;22:7297–7307. [PubMed: 12177225]

Oberheim NA, Tian GF, Han X, Peng W, Takano T, Ransom B, et al. Loss of astrocytic domain organization in the epileptic brain. Journal of Neuroscience 2008;28(13):3264–3276. [PubMed: 18367594]

Parpura V, Haydon PG. Physiological astrocytic calcium levels stimulate glutamate release to modulate adjacent neurons. Proceedings of the National Academy of Sciences of the United States of America 2000;97:8629–8634. [PubMed: 10900020]

Parpura V, Basarsky TA, Liu F, Jeftinija K, Jeftinija S, Haydon PG. Glutamate-mediated astrocyte–neuron signalling. Nature 1994;369(6483):744–747. [PubMed: 7911978]

Perez-Velazquez JL, Carlen PL. Synchronization of GABAergic interneuronal networks during seizure-like activity in the rat horizontal hippocampal slice. European Journal of Neuroscience 1999;11:4110–4118. [PubMed: 10583499]

Pinto DJ, Patrick SL, Huang WC, Connors BW. Initiation, propagation, and termination of epileptiform activity in rodent neocortex *in vitro* involve distinct mechanisms. Journal of Neuroscience 2005;25 (36):8131–8140. [PubMed: 16148221]

Rainer G, Asaad WF, Miller EK. Memory fields of neurons in the primate prefrontal cortex. Proceedings of the National Academy of Sciences of the United States of America 1998;95:15008–15013. [PubMed: 9844006]

Romo R, Brody CD, Hernandez A, Lemus L. Neuronal correlates of parametric working memory in the prefrontal cortex. Nature 1999;399(6735):470–473. [PubMed: 10365959]

Sanchez-Vives MV, McCormick DA. Cellular and network mechanisms of rhythmic recurrent activity in neocortex. Nature Neuroscience 2000;3:1027–1034.

Schiff SJ, Sauer T, Kumar R, Weinstein SL. Neuronal spatiotemporal pattern discrimination: The dynamical evolution of seizures. NeuroImage 2005;28:1043–1055. [PubMed: 16198127]

Shu Y, Hasenstaub A, McCormick DA. Turning on and off recurrent balanced cortical activity. Nature 2003;423(6937):288–293. [PubMed: 12748642]

Soltesz, I.; Staley, K. Computational neuroscience in epilepsy. Amsterdam: Academic; 2008.

Somjen, GG. Ions in the brain: normal function, seizures, and stoke. Oxford: Oxford University Press; 2004.

Tian GF, Azmi H, Takano T, Xu Q, Peng W, Lin J, et al. An astrocytic basis of epilepsy. Nature Medicine 2005;11(9):973–981.

Trevelyan AJ, Sussillo D, Watson BO, Yuste R. Modular propagation of epileptiform activity: Evidence for an inhibitory veto in neocortex. Journal of Neuroscience 2006;26(48):12447–12455. [PubMed: 17135406]

Turrigiano GG. The self-tuning neuron: Synaptic scaling of excitatory synapses. Cell 2008;135:422–435. [PubMed: 18984155]

Van Vreeswijk C, Sompolinsky H. Chaos in neuronal networks with balanced excitatory and inhibitory activity. Science 1996;274(5293):1724–1726. [PubMed: 8939866]

Vogels TP, Rajan K, Abbott LF. Neural network dynamics. Annual Review of Neuroscience 2005;28:357–376.

Wang XJ. Calcium coding and adaptive temporal computation in cortical pyramidal neurons. Journal of Neurophysiology 1998;79(3):1549–1566. [PubMed: 9497431]

Wang XJ. Synaptic basis of cortical persistent activity: the importance of NMDA receptors to working memory. Journal of Neuroscience 1999;19(21):9587–9603. [PubMed: 10531461]

Wang XJ. Persistent neuronal activity: Experiments and theory. Cerebral Cortex 2003;13:1123. [PubMed: 14576204]

Ziburkus J, Cressman JR, Barreto E, Schiff SJ. Interneuron and pyramidal cell interplay during *in vitro* seizure-like events. Journal of Neurophysiology 2006;95:3948–3954. [PubMed: 16554499]
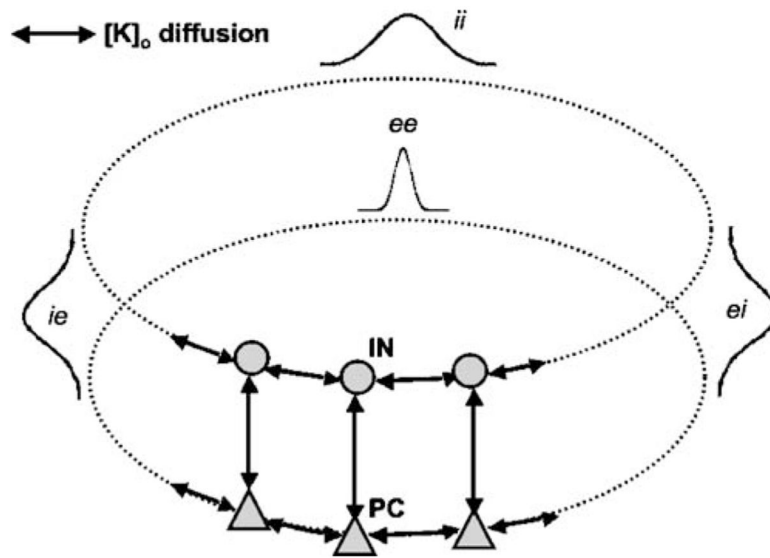
Fig. 1.
Topology of the network. The network consists of one pyramidal cell layer and one interneuron layer, both arranged in a ring (*dotted lines*). The two neuronal types make synaptic connections in the same layer as well as across the layers with Gaussian synaptic footprints (represented by Gaussian curves, where *ee*, *ei*, *ie*, and *ii* stand for excitatory–excitatory, excitatory–inhibitory, inhibitory–excitatory, and inhibitory–inhibitory synaptic connections respectively). The narrower *ee* Gaussian curve indicates that excitatory neurons make more spatially localized synaptic connections to other excitatory neurons (see "Methods" section). The K$^+$ concentration around each neuron diffuses to the nearest neighbors in the same layer and the nearest neighbor in the next layer (represented by *solid lines* with *double arrows*)
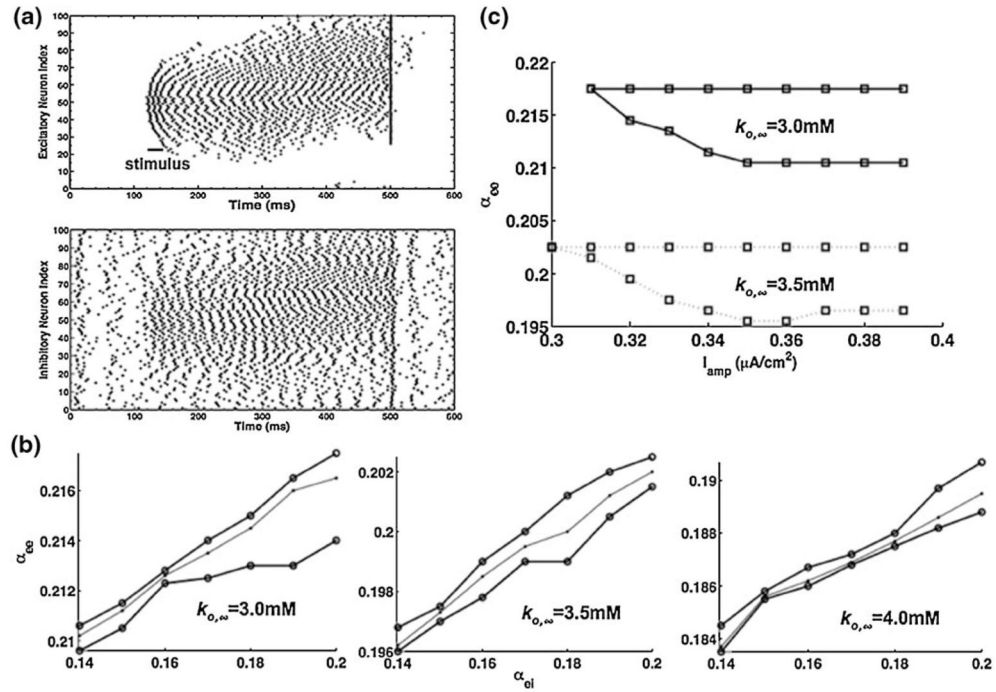
Fig. 2.
The existence and stability of spatially restricted foci of activity in our neuronal network. (**a**) A 20 ms excitatory Gaussian stimulus with amplitude I_{amp} =1.5 μA/cm^2 (see text) applied to PCs 21–79 causes a persistent and spatially restricted activity packet in the network. This activity is turned off by synchronizing neuronal activity using a strong 1 ms stimulus of 100 μA/cm^2 at t=500 ms. The *top* (*bottom*) *panel* shows a raster plot for the PC (IN) network where each *dot* represents a single-cell spike in the network. Here α_{ee}=0.215, and $k_{o,\infty}$=3.0 mM. (**b**) The region for persistent and spatially restricted focus of activity using three different $k_{o,\infty}$ values. The focus is persistent, spatially restricted and is turned off by a strong synchronizing stimulus in the region enclosed by *two lines* (*thick solid lines* with *circles* for three $k_{o,\infty}$ values). Below this region the inhibition is stronger than excitation and the focus does not exist, while above this region the excitation is stronger as compared to inhibition and the activity spreads throughout the entire network. The α_{ee} values for a stable activity focus decreases as $k_{o,\infty}$ is increased ((**b**), *middle* and *right panels*) showing that for persistent states, the increase in $k_{o,\infty}$, must be balanced by a decrease in excitation (note the different ordinate scales). The *thin solid lines* with bullets inside all activity regions represent the upper bound of the activity regions that are stable against perturbations of fixed (moderate) size. i.e. if the network is between the lower bound of the activity region and the *thin line* with *bullets*, then the network is stable against moderate perturbations. Above the *thin line* in each region the network can show persistent and spatially restricted foci of activity but is not stable against moderate perturbations (although it is still stable against small perturbations). It is clear that the percentage of the activity region that is stable to perturbations decreases with increasing $k_{o,\infty}$. The existence of the focus also depends on the stimulus strength. The focus does not exist if the stimulus is too weak (**c**). After a certain threshold of the stimulus (I_{amp} =0.31 here) the weakness of the stimulus is compensated by the excitation strength and external potassium level. A value of α_{ei} =0.2 is used for simulations in (**a**), (**c**)
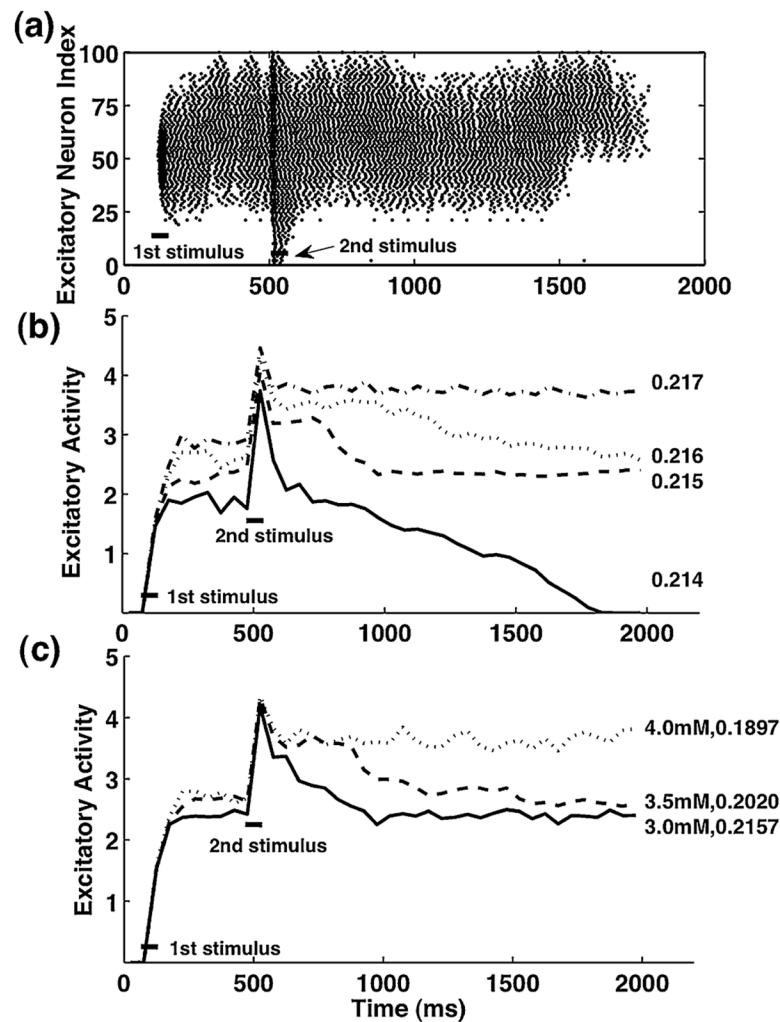
Fig. 3.
The activity (see text for definition) of the excitatory population for various α_{ee} values. The first stimulus (see text) at $t = 112$ ms for 20 ms causes a stable focus of activity in the network. A second stimulus of 1.0 µA/cm^2 at $t=500$ ms for 20 ms causes the focus to take over the entire population. After the stimulus is removed the network either decays to the zero-activity state, returns to the stable focus or remains in the state where activity is spread throughout the entire population depending on the excitation strength. In (**a**) we show a raster plot for a single simulation where the activity decays to zero after the perturbation. $\alpha_{ee}=0.214$ is used in this example. (**b**) Network activity for different α_{ee} values. The *numbers* on the *right* of each *line* are the α_{ee} values used during the simulations. (**c**) Same as (**b**) but here we use the different $k_{o,\infty}$ values given in the plot. The stability of the network also depends on the steady state $[K]_o$. For smaller extracellular K$^+$ the network activity decays back to the stable focus after the second stimulus is turned off. However, if $[K]_o$ is high the network maintains its enhanced activity even after the second stimulus vanishes. α_{ee} values are chosen such that they lie at the centers of the activity regions shown in Fig. 2(b) (*right column* in Fig. 3(c)). For all simulations in (**a**)–(**c**) $\alpha_{ei} =0.2$ is used. The *curves* in *panels* (**b**) and (**c**) are averaged over several trials
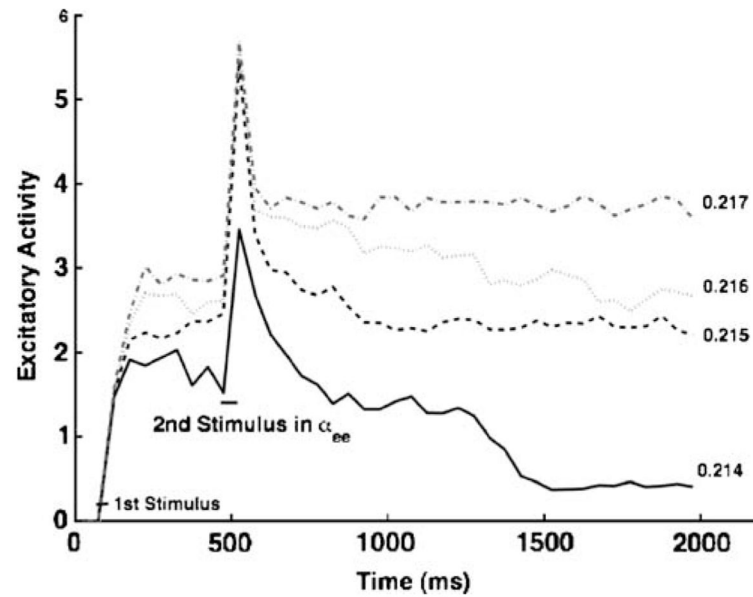
Fig. 4.
Same as Fig. 3(b),(c) but the second stimulus is in α_{ee}, i.e. instead of applying current for the second stimulus the α_{ee} is increased beyond the stable activity region (see Fig. 2(b)) to a value of 0.25 for 30 ms at t=500 ms. After the α_{ee} value is restored the network returns to the stable focus of activity if the baseline α_{ee} is in an intermediate range. If the baseline α_{ee} is too large the network cannot return to the stable focus. Similarly if the baseline α_{ee} is too small the persistent state decays after the perturbation is removed. The baseline α_{ee} values are given in the plot and α_{ei} =0.2
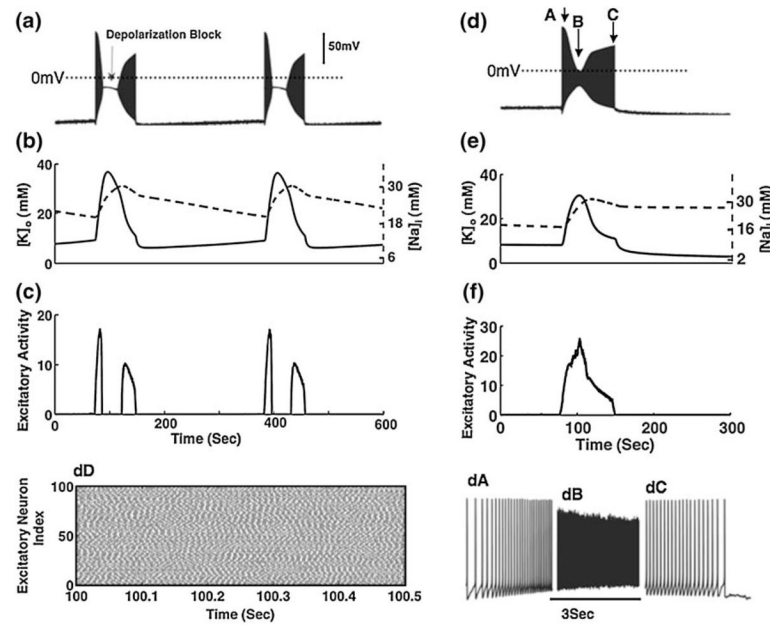
Fig. 5.
Spontaneous activity in the network for varying $[K]_o$. In panel (**a**) we show the membrane potential of one PC in the network as (**b**) $[K]_o$ (*solid line*) and $[Na]_i$ (*dashed line*) evolve in time. (**c**) shows the activity of the network, where the drop in activity occurs at high $[K]_o$ values due to the switching of the network to depolarization block. For (**a**)–(**c**) G_{glia} =16.7 *and* ε =0.23. In (**d**)–(**f**) we repeat the simulations in (**a**)–(**c**) using G_{glia} =26.7 *and* ε =0.003. For these parameters all cells in the network show high frequency seizure-like firing for higher $[K]_o$ values instead of going into depolarization block. As is clear from (*dA*) each cell exhibits regular spiking initially but shifts to seizure-like bursting for higher $[K]_o$ values (*dB*), and finally to a silent state (end of *dC*). There is a clear peak in the activity of the network at high $[K]_o$ values, indicating the increased synchrony in the network (**f**). The raster plot at peak activity is shown in (*dD*). The *solid* and *dashed lines* in (**e**) show $[K]_o$ and $[Na]_i$ trajectories respectively for the PC shown in (**d**). Parameter values used for simulation in this figure are $k_{o,\infty}$ =14 mM, α_{ee} =0.12, and α_{ei} =0.2

Table 1

Model variables and parameters

	Description
Variable	
V	Membrane potential
I_K	Potassium current
I_{Na}	Sodium current
I_L	Leak current
I_{syn}	Synaptic current
I_{ext}	Stimulus current
I_{rand}	Random background noise
s	Variable giving the temporal evolution of synapse
V_L	Reversal potential of leak current
I_{pump}	Pump current
I_{glia}	Glial uptake
$[K]_o$	Extracellular potassium concentration
$[K]_i$	Intracellular potassium concentration
g^{ij}	Spatial extent of synaptic current from ith to jth neuron
χ	Variable modeling the depolarization block
η	Threshold to synaptic block due to the depolarization
$[Na]_o$	Extracellular sodium concentration
$[Na]_i$	Intracellular sodium concentration
Parameter	
C	Membrane capacitance
I_{amp}	Stimulus amplitude
τ	Time constant of synapses
g_L	Conductance of leak current
g_{AHP}	Conductance of afterhyperpolarization current
$k_{o,\infty}$	Steady state extracellular potassium concentration
G_{glia}	Strength of glial uptake
α_{ij}	Strength of synaptic current from ith to jth neuron
ε	Constant for potassium diffusion to bath solution
γ	Forward rate constant into and out of synaptic block due to depolarization
$\bar{\gamma}$	Backward rate constant into and out of synaptic block due to depolarization
D	Diffusion coefficient of potassium
$[Cl]_o$	Extracellular chloride concentration
$[Cl]_i$	Intracellular chloride concentration